CHEMISTRY
A EUROPEAN JOURNAL

ChemPubSoc
Europe

DOI: 10.1002/chem.201301825

Synthesis and Structural Characterization of Hexacoordinate Silicon, Germanium, and Titanium Complexes of the *E. coli* Siderophore Enterobactin

Todor Baramov,[a] Karlijn Keijzer,[b] Elisabeth Irran,[a] Eva Mösker,[a] Mu-Hyun Baik,*[b, c] and Roderich Süssmuth*[a]

Abstract: The *E. coli* siderophore enterobactin, one of the strongest Fe^{III} chelators known to date, is also capable of binding Si^{IV} under physiological conditions. We report on the synthesis and structural characterization of the tris(catecholate) Si^{IV}–enterobactin complex and its Ge^{IV} and Ti^{IV} analogues. Comparative structural analysis, supported by quantum-chemical calculations, reveals the correlation between the ionic radius and the structural changes in enterobactin upon complexation.

Keywords: enterobactin · germanium · siderophores · silicon · titanium

Introduction

Iron is the fourth most abundant element on Earth, but it is not readily bio-available due to the low solubility of Fe^{III} salts at neutral and basic pH. In response, bacteria evolved iron extraction strategies using siderophores, which are low-molecular weight chelating agents that exhibit high Fe^{III}-binding affinities.[1] For example, enteric bacteria such as *E. coli* and *Salmonellae* produce the hexadentate enterobactin (Ent, **1**), which is considered to be the strongest ferric chelator with an estimated K_d as low as 10^{-49} M (Scheme 1).[2] Its triseryl macrolactone backbone bears three 2,3-dihydroxybenzoyl (Dhb) residues that become catecholate ligands after deprotonation to form an octahedral hexacoordinate high-spin Fe^{III} complex.[2] Despite significant efforts, the structure of the Fe^{III}–Ent complex has not been determined successfully to date. The only crystal structure of a metal–enterobactin complex available is the V^{IV}–Ent complex, which is commonly used as a model for the structure of Fe^{III}–Ent.[3] Although the main biological function of enterobactin is to effectively transport Fe^{III}, it was found to bind many other metal ions with varying affinities.[4] Recently, we found that Ent binds silicon to form the hexacoordinate complex Si^{IV}–Ent (**2a**) at physiological pH,[5] representing the first example of a natural product bound to silicon under physiological conditions, which makes it an interesting model for comparison with other hexacoordinate silicon complexes.[6] Along with the interest in higher coordinate silicon compounds, many studies have focused on the synthesis and characterization of hexacoordinate catecholate germanium and titanium complexes.[7–9] Attachment of enterobactin and other catecholate-type compounds to oxidic surfaces, for example, TiO_2 is of interest with respect to bacterial biofilm formation, generation of antimicrobial surfaces, and immobilization of catalysts.[9c–e]

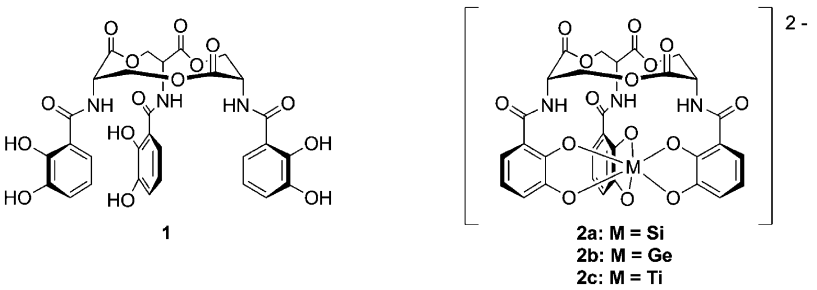

Scheme 1. Structure formulae of enterobactin **1** (Ent) and its Si, Ge, and Ti complexes **2a**, **2b**, and **2c**.

Herein, we present the synthesis and X-ray crystallographic analysis of the silicon (**2a**), germanium (**2b**), and ti-

[a] T. Baramov, Dr. E. Irran, E. Mösker, Prof. Dr. R. Süssmuth
Technische Universität Berlin, Fakultät II, Institut für Chemie
Strasse des 17. Juni 124, 10623 Berlin (Germany)
Fax: (+49) 30-314-79651
E-mail: suessmuth@chem.tu-berlin.de

[b] K. Keijzer, Prof. Dr. M.-H. Baik
Department of Chemistry
Indiana University, Bloomington, IN 47405 (USA)
E-mail: mbaik@indiana.edu

[c] Prof. Dr. M.-H. Baik
Department of Materials Chemistry, Korea University
Jochiwon-eup, Sejong-si, 339-700 (South Korea)

Supporting information for this article is available on the WWW under http://dx.doi.org/10.1002/chem.201301825.

tanium (**2c**) complexes of enterobactin. By comparing the M–Ent interactions, taking into account the rigidity of the triseryl macrolactone ring[3] and alternating the metal, we derived trends for the binding properties. To obtain a more detailed understanding, we carried out a series of quantum-chemical model calculations, which allowed for correlating the effective ionic radius[10] of the metal, structural changes in the corresponding M–Ent complex, and the computed binding energies. Si^{IV} is the smallest cation known to bind to enterobactin. The metal unspecific binding behavior of Ent is interesting and offers a unique opportunity for studying the chemical behavior of Ent in detail. Silicon lacks unpaired valence electrons and low-energy, electronically excited states that continue to make mechanistic work on Fe-binding difficult. Thus, we anticipate that silicon binding will provide a convenient platform for studying how Ent binds highly charged metal ions. Given the radically different electronic features between silicon and iron, we suspect that the silicon binding may be notably different from iron binding. A promising way of understanding these differences is our combined experimental and computational approach. Ti^{IV}–Ent is an important member in our systematic study, as the Ti^{IV} d^0 center lacks unpaired valence electrons, as does silicon, but it can access d-orbitals that will be important in Fe^{III}–Ent. In addition, Ti^{IV}–Ent should in principle be a better model for Fe^{III}–Ent than V^{IV}–Ent that was studied previously, as the ionic radius of Ti^{IV} is a closer to that of iron.[10]

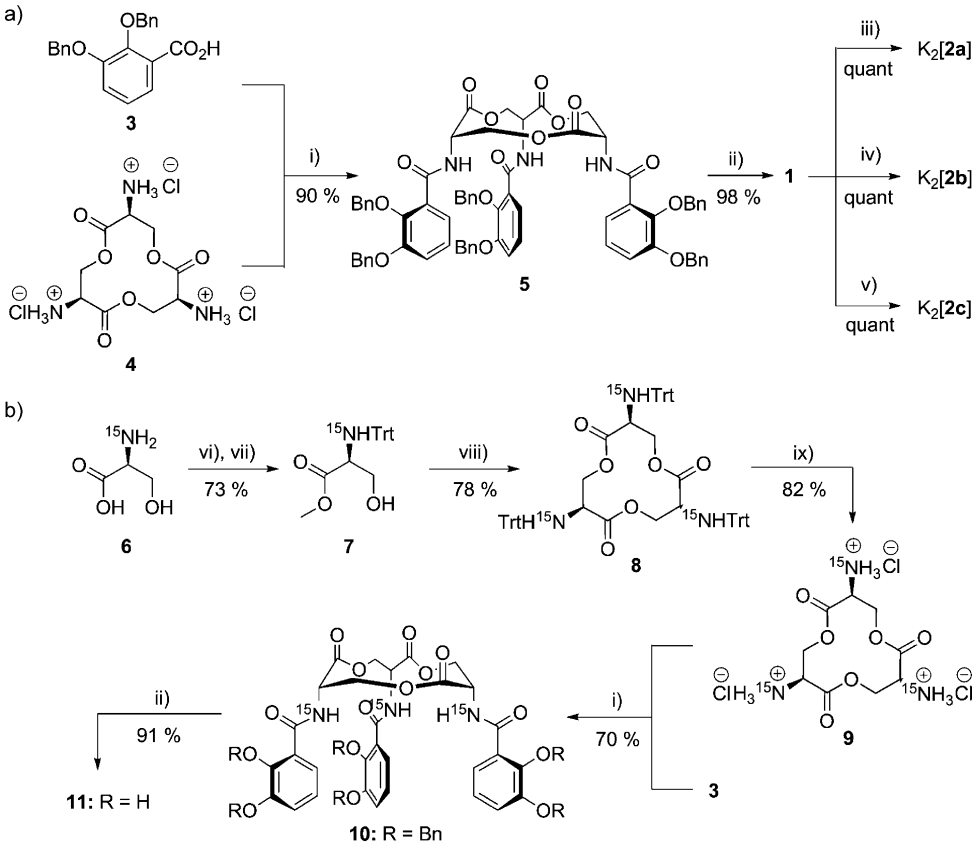

Scheme 2. a) Synthesis of compound **1** and of the potassium salts of **2a–c**: i) DIC, HOBt, Et_3N, CH_2Cl_2, RT, ii) H_2, Pd/C, EtOAc, EtOH, iii) $Si(OMe)_4$, KOH, MeOH, RT, iv) $Ge(OMe)_4$, KOH, MeOH, RT, v) $Ti(OiPr)_4$, KOH, MeOH, RT. b) Synthesis of ^{15}N-labeled enterobactin **11**: vi) MeOH, $SOCl_2$, RT; vii) TrtCl, Et_3N, DCM, RT, viii) stannoxane, *m*-xylene, reflux, ix) 1.5 M HCl/EtOH, reflux. DIC = N,N′-diisopropylcarbodiimide, HOBt = 1-hyroxybenzotriazole.

Results and Discussion

Enterobactin **1** was synthesized from acid **3**[11] in two steps (Scheme 2). The macrocyclic lactone salt **4** was prepared according to previously published protocols.[12a] Coupling of **4** to benzyl-protected acid **3** by means of DIC/HOBt provided the fully protected enterobactin **5** in 90% yield. These coupling conditions resulted in higher yields compared to previously described procedures employing acid chlorides, in which the maximal reported yield was 79%.[12] Compound **5** was transformed into Ent **1** by hydrogenolysis.[12]

Treatment of enterobactin with $Si(OMe)_4$, $Ge(OMe)_4$, and $Ti(OiPr)_4$ in the presence of a stoichiometric amount of KOH provided the potassium salts of **2a–c** in quantitative yields. This synthetic protocol enabled the preparation of the Si, Ge, and Ti complexes by a simple purification procedure. High-resolution ESI-MS, as well as ^1H and ^{13}C NMR spectra of **2a–c** (see Supporting Information) reveal comparable sets of signals and are in support of the corresponding structures of **2a**, **2b**, and **2c** (Scheme 2). The NMR spectra confirmed the presence of intramolecular hydrogen bonding between the amide protons and the *ortho* catecholate oxygen atoms in the complexes (Figure 1).

To study the reactions of enterobactin with Si, Ge, and Ti, time-dependent NMR studies were performed. As we showed previously, Ent reacts with $Si(OMe)_4$ even without addition of base to afford the protonated form H_2[**2a**].[5] To compare the rate of formation of **2a–c**, three NMR experiments were performed (see the Supporting Information). Solutions of **1** in [D_6]DMSO were treated with $Si(OMe)_4$, $Ge(OMe)_4$, and $Ti(OiPr)_4$, respectively. The formation of the Ge^{IV}–Ent and Ti^{IV}–Ent complexes was completed within 1 h, whereas Si^{IV}–Ent was formed within 24 h.

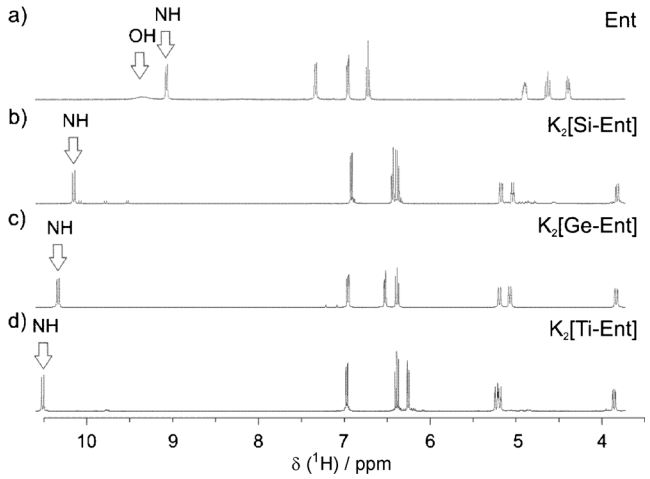

Figure 1. Comparison between the ^{1}H NMR spectra (400.1 MHz) of enterobactin and the potassium salts of **2a** (Si^{IV}–Ent), **2b** (Ge^{IV}–Ent), and **2c** (Ti^{IV}–Ent) in [D_6]DMSO.

Complexes **2a–c** were crystallized from DMF/Et_2O yielding K_2[Si–Ent]·4 DMF·Et_2O·H_2O, K_2[Ge–Ent]·6 DMF·H_2O, and K_2[Ti–Ent]·3 DMF, respectively (see the Supporting Information).[13] Complexes **2a** and **2b** crystallized in the space group $P2_12_12_1$, whereas **2c** crystallized in space group $P2_1$. The high-resolution structures (Figure 2) reveal that the metal ions are coordinated to the catechol moieties. All three complex anions (**2a–c**) display twisted octahedral geometry, approximate C_3 point symmetry, and Δ configuration of the metal centers, which is in good agreement with the previously characterized V^{IV}–Ent complex.[3] Our quantum-chemical simulations reliably reproduce all crystal structures (Figure 2 d).

As seen from the single-crystal structures of Si^{IV}–Ent, Ge^{IV}–Ent, and Ti^{IV}–Ent, the chirality of the L-serines uniformly induces complexes with Δ configuration at the metal centers. This is consistent with the Δ absolute configuration of the Fe^{III}–, Cr^{III}–, and Rh^{III}–Ent complexes, which was confirmed by CD spectroscopy.[14] It was previously demonstrated that the Δ configuration of Fe^{III}–Ent is crucial for the biological activity of the siderophore.[15] Our findings support the notion that the stereochemistry is primarily determined by the chirality of the L-serine base. Comparison of the Si^{IV}–, Ge^{IV}–, and Ti^{IV}–Ent complexes with the X-ray structure of the V^{IV}–Ent complex[3] can provide insights into important molecular features relevant for Fe^{III} chelation by enterobactin. Among all four metals, Si^{IV} (0.40 Å) has the smallest ionic radius compared to Ge^{IV} (0.53 Å), V^{IV} (0.58 Å), and Ti^{IV} (0.61 Å).[10]

The crystallographic data reveals that the main differences in the structures are in the M–O distances (Table 1) and the dihedral angle C8-N1-C7-O3 (Table 2). Si^{IV}–Ent has the shortest and Ti^{IV}–Ent the longest M–O bonds, which is consistent with the differences in the ionic radii. The distance between the metal and the *ortho* catechol oxygen (M–O1) is generally longer than the distance between the metal and the *meta* catechol oxygen (M–O2). The bite angle (O1-M-O2) for Si^{IV}–Ent is 86.8(2)°, whereas the Ti^{IV}–Ent complex has a bite angle of 78.9(2)° caused by the larger effective radius of Ti^{IV}. Hence short M–O distances, caused by relative small ionic radius of M, give rise to larger bite angles

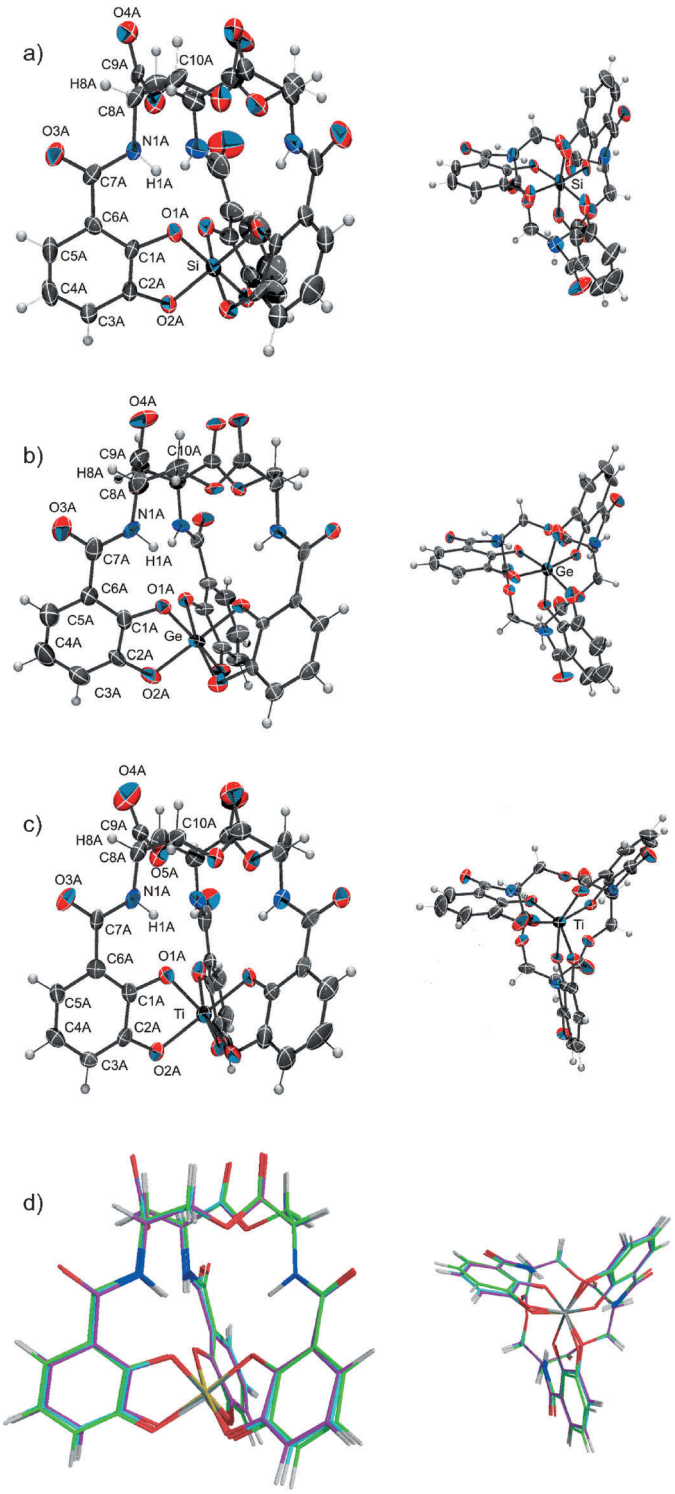

Figure 2. Side (left) and bottom (right) views of the molecular structures in the crystals of a) Si^{IV}–Ent **2a**, b) Ge^{IV}–Ent **2b** and c) Ti^{IV}–Ent **2c** (probability level of displacement ellipsoids 50%), d) overlay of the calculated structures of Si^{IV}–Ent (magenta), Ge^{IV}–Ent (blue), and Ti^{IV}–Ent (green).

Table 1. Comparison between selected average bond lengths [Å] in the structures of the Si^{IV}–, Ge^{IV}–, V^{IV}–, and Ti^{IV}–enterobactin complexes. For the torsion angles the absolute values are given.

Bond	Si^{IV}–Ent	Ge^{IV}–Ent	V^{IV}–Ent[a]	Ti^{IV}–Ent
M[b]–O1	1.785(5)	1.899(5)	1.946(3)	1.983(6)
M[b]–O2	1.771(6)	1.879(5)	1.939(3)	1.954(6)
C8–C9	1.529(11)	1.523(11)	1.537	1.518(13)
C8–C10	1.486(11)	1.521(11)	1.498	1.515(12)
O5–C9	1.345(10)	1.333(9)	1.341	1.317(10)
O5–C10	1.467(9)	1.449(9)	1.457	1.452(10)

[a] Data as published by Raymond et al.[3] [b] M = Si, Ge, V, Ti.

Table 2. Comparison between selected average bond angles [°] in the structures of the Si^{IV}–, Ge^{IV}–, V^{IV}–, and Ti^{IV}–enterobactin complexes. For the torsion angles the absolute values are given.

Angle	Si^{IV}–Ent	Ge^{IV}–Ent	V^{IV}–Ent[a]	Ti^{IV}–Ent
O1-M[b]-O2	86.8(2)	85.5(2)	79.8(1)	78.9(2)
M[b]-O1-C1	113.0(4)	111.2(4)	116.3(3)	116.0(5)
M[b]-O2-C2	113.7(5)	111.6(5)	115.6(3)	116.9(5)
C9-C8-C10-O5	66.4(8)	66.7(8)	67.0	65.1(10)
C10-O5-C9-C8	175.2(7)	179.4(7)	175.9	176.1(7)
C8-N1-C7-O3	13.6(12)	11.1(13)	4.0	3.7(13)

[a] Data as published by Raymond et al.[3] [b] M = Si, Ge, V, Ti.

(Table 2). The dihedral angle of the amide bond which should be close to 0° is 13.6(12)° in the Si^{IV}–Ent and 3.7(13) in Ti^{IV}–Ent (Table 2). The effective ionic radius of Ti^{IV} is the closest to the ionic radius of Fe^{III} (0.65 Å) and therefore the structure of Ti^{IV}–Ent is expected to best approximate the structure of the Fe^{III}–Ent. Taking into account these observations it could be expected that the C8-N1-C7-O3 angle would be closer to 0° in Fe^{III}–Ent.

Previous experimental studies on ferric binding by enterobactin and its analogues, demonstrated that substitution of the macrolactone ring for platforms with different flexibility affects the binding affinity of the ligand due to steric constrains.[16a–d] In addition, molecular mechanics studies comparing Fe^{III} binding by different (synthetic) enterobactin analogues[16f] showed that the structural distortion that is caused upon binding a metal to enterobactin can be separated into two components: i) the amount of distortion imposed on the ligand characterized by the change of the triseryl-backbone structure from its equilibrium geometry and ii) the amount of distortion in the immediate coordination sphere of the metal enforced by the structural rigidity of Ent.[16] The latter is interesting, as it quantifies the effect of tethering three catechol ligands within the Ent structure and can be assessed by comparing the geometry of the catechols around the metal in the M–Ent complex with the geometry the metal would adopt if they were not restrained by a backbone, that is, a metal bound to three free catechol ligands. The most favorable M–Ent complex should have 1) a minimal distortion of the backbone and 2) minimal deviation from the preferred coordination geometry specific to the metal.

To quantify these trends, we used our quantum-chemically calculated structures to first determine the root mean square deviation (RMSD) between the various metal-bound structures. The distortion of the backbone is directly proportional to the radius of the metal ion following the trend Si < Ge < Ti (Table 3). The distortion in the backbone is most severe for the Ti^{IV}–Ent complex with the RMSD(backbone)

Table 3. Comparison of the structural distortions imposed on binding Si, Ge, and Ti to enterobactin.

Complex	RMSD(cavity) [Å]	RMSD(backbone) [Å]
$[Si–Ent]^{2-}$	0.177	0.275
$[Ge–Ent]^{2-}$	0.253	0.299
$[Ti–Ent]^{2-}$	5.84×10^{-5}	0.324

being 0.324 Å. Interestingly, the binding cavity structure for Ti^{IV} is closest to what it would prefer when bound to three free catechol ligands with the RMSD(cavity) being practically zero (5.84×10^{-5} Å). In contrast, the binding geometry that Ent offers to Ge^{IV} is the least favorable in the series with an RMSD(cavity) of 0.253 Å (Table 3). The RMSD for the binding cavity of Si is smaller than for Ge, which is easy to understand: As Si–O bonds are stronger than Ge–O bonds, Si should be more effective in enforcing a binding cavity geometry that is structurally closer to what it prefers if the catecholates were not restrained by the backbone. These results are supported by a comparison of the crystal structures of $Si^{IV}(cat)_3$[17] and $Ti^{IV}(cat)_3$[18] with Si^{IV}–Ent and Ti^{IV}–Ent, respectively. The values of the bite angles and the average M–O distances in $Ti^{IV}(cat)_3$ and Ti^{IV}–Ent are closer compared to the corresponding parameters for $Si^{IV}(cat)_3$ and Si^{IV}–Ent (Table 4). In summary, distortions in the backbone

Table 4. Comparison between average M–O bond lengths [Å] and bite angles [°] in the structures of $M(cat)_3$[17a,18] and M–Ent.

Parameter	Si^{IV} $(cat)_3$[b]	Si^{IV}–Ent	Δ	$Ti^{IV}(cat)_3$[c]	Ti^{IV}–Ent	Δ
M[a]-O	1.784(3)	1.778(6)	0.006	1.966(27)	1.968(6)	0.002
O-M[a]-O	88.6(0.2)	86.8(2)	1.8	80.3(2)	78.9(2)	1.4

[a] M = Si, Ti. [b] Data as published by Boer et al.[17a] [c] Data as published by Raymond et al.[18]

of enterobactin caused by metal-binding are small and are only slightly affected by the type of cation that is bound. In general, smaller ions give less distortion. The main energetic contribution to complex formation originates from the capability of enterobactin to provide a coordination geometry of the catechol ligands around the metal that maximizes the electronic M–O interactions, which is also dependent on the ability of the metal to enforce such a binding cavity.

Figure 3 summarizes the quantum-chemically calculated energies for the metal-binding process. Our calculations indicate that electronically,[19] Ti^{IV} binding is 72 and 156 kcal mol^{-1} more favorable than Si^{IV} and Ge^{IV}, respectively (Figure 3a).[20] These energies are in good agreement with the expectation that the octahedral, six-coordinate binding site in Ent is most suited to bind transition metals that can utilize d-orbitals in addition to the s and p orbitals to form M–O σ bonds. Between the main group metals, Si will from

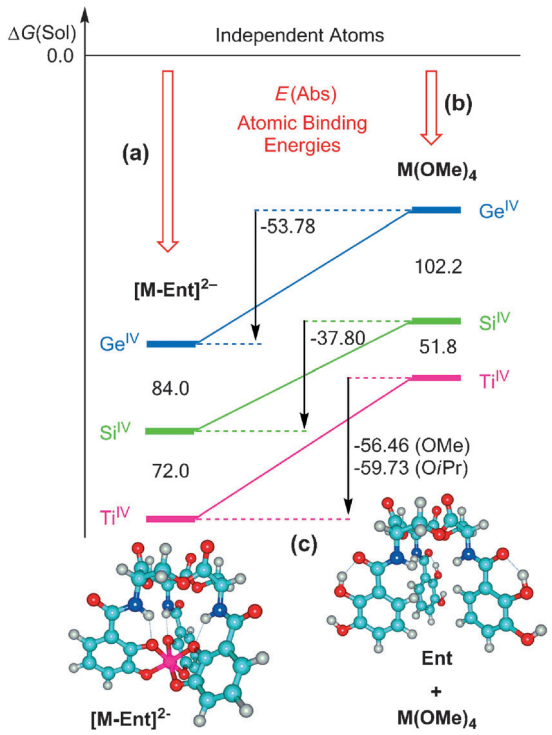

Figure 3. Qualitative picture of the reaction profile for formation of M–Ent complexes. Si^{IV}–Ent gives the smallest ΔG(Sol) [kcal mol^{-1}] in DMSO.

stronger bonds, as Si^{IV} is a harder Lewis acid than Ge^{IV} making it a better binding partner for the relatively hard O-based Lewis bases. To understand the metal-binding experiments mentioned above, we must consider that the metal ions initially exist as complexes of $M(OMe)_4$.[21] Thus, the experimental observations depend not only on the M–Ent binding, but also on the M–OMe bond cleavage (Figure 3b). The M–O binding preference of Si^{IV} over Ge^{IV} is even more pronounced in the methoxy complex with an electronic binding energy difference of 102 kcal mol^{-1}. As a consequence, the overall gain in solution phase free energy ΔG(sol) for the reaction is smaller for Si^{IV} than for Ge^{IV} (Figure 3c). The favorable binding energy for Si^{IV} on the reactant side (Figure 3b) also explains the slow kinetics observed in the experiment, since it will be harder to break the Si–O bonds in $Si(OMe)_4$ compared to the Ge–O bonds in $Ge(OMe)_4$.

To experimentally estimate the thermodynamic and kinetic properties of compounds **2a–c** compared to the V^{IV}–, Ga^{III}–, and Fe^{III}–Ent complexes, they were prepared as triethylammonium salts and their formation was controlled by ESI-MS and CD spectroscopy (see the Supporting Information). ^{15}N-labeled enterobactin-probe **11** was synthesized from ^{15}N-labeled serine **6** in six steps (Scheme 2) and subjected to an exchange reaction with M–Ent complexes (M = Si, Ge, Ti, V, Fe, Ga) monitored by ESI-MS (see the Supporting Information). Stoichiometric amounts of the labeled ligand were incubated with the M–Ent complexes for 24 h in methanolic and aqueous solutions. Fe^{III}– and Ga^{III}–Ent are labile with respect to Ent exchange in both aqueous and methanolic solutions and formation of ^{15}N-labeled Ent complexes is observed. In contrast, no exchange is detected for the Si^{IV}–, Ge^{IV}–, Ti^{IV}–, and V^{IV}–Ent complexes. These results are in agreement with the previously stated kinetic lability of Fe–siderophore complexes due to the high-spin d^5 configuration of the ferric ion, which places electrons in M–L antibonding orbitals that assist M–L bond cleavage reactions.[22] It is therefore not surprising that crystallization of Ent complexes has been achieved only with the elements, which form kinetically inert complexes.

To assess whether or not M–binding is reversible, the above mentioned M–Ent complexes (M = Si, Ge, Ti, V, Fe, Ga) were each treated with $Si(OMe)_4$, $Ge(OMe)_4$, $Ti(OiPr)_4$, and $Fe(acac)_3$ solutions and incubated for 24 h at room temperature (see the Supporting Information). Similarly to our previous observations for Si^{IV}–Ent and Si^{IV}–Sal,[5] all six complexes were stable in aqueous solution and no exchange of the bound metal could be detected, suggesting that the M–Ent binding is irreversible under normal conditions. However, the Fe^{III}– and Ga^{III}–Ent complexes could be converted into the corresponding Ge^{IV}– and Ti^{IV}–Ent complexes upon treatment with $Ge(OMe)_4$ and $Ti(OiPr)_4$ in MeOH. Moreover the conversion of the Fe^{III}–Ent into Ti^{IV}–Ent could be monitored by time-dependent CD spectroscopy (Figure 4). This remarkable observation can be understood considering that the electrostatic interaction of Fe^{III} and Ga^{III} with the polyanionic ligand is much smaller than for Ge^{IV} and Ti^{IV}. Replacement of the 3+ metals with the 4+ metals is irreversible and neither Fe^{III} nor Ga^{III} are able to displace Ge^{IV} or Ti^{IV}. As the solvation energy differences between the 3+ and 4+ cations are expected to be less pronounced in the lower dielectric medium, it is understandable that these metal-exchange reactions are seen in methanol, but not in water.

Conclusion

The characterization of the Si^{IV}–, Ge^{IV}–, and Ti^{IV}–Ent complexes presented herein facilitates comparative studies of Ent complexes with different metals. Our studies give insights into structural changes of Ent upon binding of metals that have different ionic radii. The kinetic inertness and the thermodynamic stability of the M–Ent (M = Si, Ge, Ti) complexes were tested by competition experiments. Quantum-chemical analysis of the M–Ent (M = Si, Ge, Ti) complexes showed that the formation of Si^{IV}–Ent is least favorable because of the high stability of the reactant, $Si(OMe)_4$, which makes the overall gain in energy for binding to enterobactin the smallest for Si^{IV}. The slow reaction kinetics of Si^{IV}–Ent is a result of the strong Si–O bonds present in the reactant complex, the lack of electrons in M–L antibonding orbitals and the 4+ charge compared to the natural binding partner Fe^{III}. These properties make Si^{IV}–Ent an excellent model to study the binding mechanism of metals by enterobactin, which is subject to our ongoing studies, as well as an interesting example of a stable hexacoordinate silicon complex.

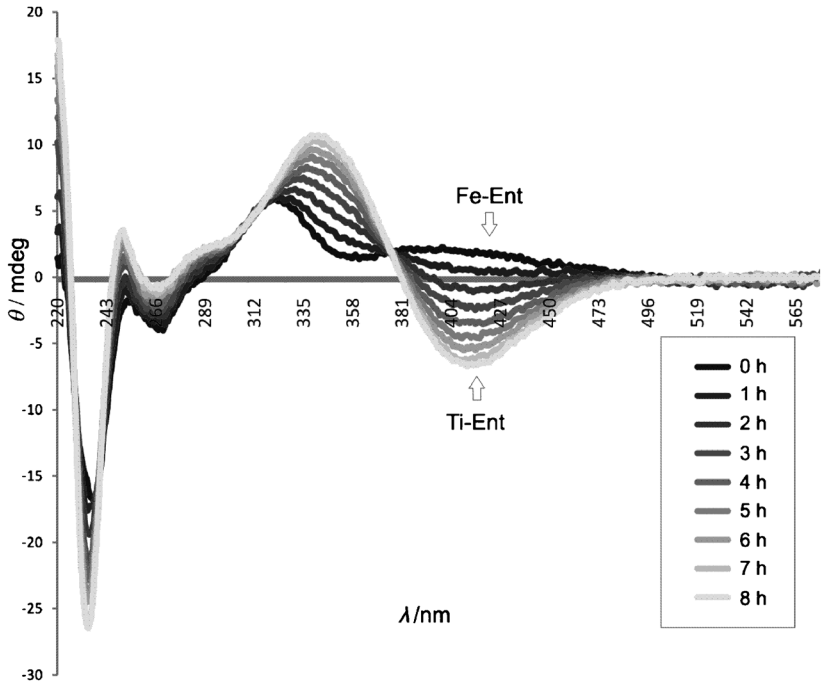

Figure 4. Conversion of Fe^{III}–Ent into Ti^{IV}–Ent, monitored by CD spectroscopy. Reaction of 0.15 mM methanolic solution of Fe^{III}–Ent (400 μL, 0.06 μmol) with 15 mM methanolic solution of Ti(O*i*Pr)$_4$ (12 μL, 0.18 μmol). After 8 h the bands at 420 and 530 nm, characteristic of Fe^{III}–Ent disappear. The absorption bands at 341 and 414 nm are indicative of Ti^{IV}–Ent. Isosbestic point at 377 nm could be observed.

Experimental Section

For full experimental details see the Supporting Information

Acknowledgements

This research was supported by grants of the Deutsche Forschungsgemeinschaft (DFG SU239/10–1) and DAAD with fellowship to T. B. We thank Dr. Sebastian Kemper, TU Berlin (Germany), and Prof. Dr. Hermen Overkleeft, Leiden University (The Netherlands), for helpful discussions. We thank the National Science Foundation (CHE-0645381), the Research Cooperation (Scialog Award) and the National Research Foundation of Korea (WCU Award R31–2012–000–10035–0) for support.

[1] R. C. Hider, X. Kong,, *Nat. Prod. Rep.* **2010**, *27*, 635–657.
[2] a) J. R. Pollack, J. B. Neilands, *Biochem. Biophys. Res. Commun.* **1970**, *38*, 989–992; b) I. G. O'Brien, F. Gibson, *Biochim. Biophys. Acta* **1970**, *215*, 393–402; c) K. N. Raymond, E. A. Dertz, S. S. Kim, *Proc. Natl. Acad. Sci. USA* **2003**, *100*, 3584–3588.
[3] a) T. B. Karpishin, K. N. Raymond, *Angew. Chem.* **1992**, *104*, 486–488; *Angew. Chem. Int. Ed. Engl.* **1992**, *31*, 466–468; b) T. B. Karpishin, T. M. Dewey, K. N. Raymond, *J. Am. Chem. Soc.* **1993**, *115*, 1842–1851.
[4] H. J. Rogers, C. Synge, V. E. Woods, *Antimicrob. Agents Chemother.* **1980**, *18*, 63–68.
[5] T. Schmiederer, S. Rausch, M. Valdebenito, Y. Mantri, E. Mösker, T. Baramov, K. Stelmaszyk, P. Schmieder, D. Butz, S. I. Müller, K. Schneider, M.-H. Baik, K. Hantke, R. D. Süssmuth, *Angew. Chem.* **2011**, *123*, 4317–4321; *Angew. Chem. Int. Ed.* **2011**, *50*, 4230–4233.
[6] O. Seiler, C. Burschka, T. Fenske, D. Troegel, R. Tacke, *Inorg. Chem.* **2007**, *46*, 5419–5424.
[7] A. Pinter, G. Haberhauer, *Chem. Eur. J.* **2008**, *14*, 11061–11068.
[8] a) A. C. Sau, R. R. Holmes, *Inorg. Chem.* **1981**, *20*, 4129–4135; b) G. Cerveau, C. Chult, R. J. P. Corriu, C. Reye, *Organometallics* **1991**, *10*, 1510–1515.
[9] a) S. Burk, M. Albrecht, K. Hiratani, *J. Inclusion Phenom. Macrocyclic Chem.* **2008**, *61*, 353–359; b) R. Uppal, H. P. Israel, C. D. Incarvito, A. M. Valentine, *Inorg. Chem.* **2009**, *48*, 10769–10779; c) H. G. Upritchard, J. Yang, P. J. Bremer, I. L. Lamont, A. J. McQuillan, *Langmuir*, **2011**, *27*, 10587–10596; d) J.-Y. Wach, S. Bonazzi, K. Gademann, *Angew. Chem.* **2008**, *120*, 7232–7235; *Angew. Chem. Int. Ed.* **2008**, *47*, 7123–7126; e) E. Franzmann, F. Khalil, C. Weidmann, M. Schröder, M. Rohnke, J. Janek, B. M. Smarsly, W. Maison, *Chem. Eur. J.* **2011**, *17*, 8596–8603.
[10] R. D. Shannon, *Acta Crystallogr. Sect. A* **1976**, *32*, 751–767.
[11] a) R. A. Gardner, R. Kinkade, C. Wang, O. Phanstiel, *J. Org. Chem.* **2004**, *69*, 3530–3537; b) J. Deng, Y. Hamada, T. Shioiri, *Synthesis* **1998**, 627–638.
[12] a) R. J. A. Ramirez, L. Karamanukyan, S. Ortiz, C. G. Gutierrez, *Tetrahedron Lett.* **1997**, *38*, 749–752; b) E. J. Corey, S. Bhattacharyya, *Tetrahedron Lett.* **1977**, *45*, 3919–3922; c) W. H. Rastetter, T. J. Erickson, M. C. Venuti, *J. Org. Chem.* **1980**, *45*, 5011–5012; d) W. H. Rastetter, T. J. Erickson, M. C. Venuti, *J. Org. Chem.* **1981**, *46*, 3579–3590; e) A. Shanzer, J. Libman, *J. Chem. Soc. Chem. Commun.* **1983**, *15*, 846–847; f) E. R. Marinez, E. K. Salmassian, T. T. Lau, C. G. Gutierrez, *J. Org. Chem.* **1996**, *61*, 3548–3550.
[13] X-ray quality crystals of the potassium salts of **2a** and **b** were grown from DMF by vapor diffusion of Et_2O at 17 °C over two weeks. Data for the single-crystal structure determination of **2a**–**c** were collected on an Oxford-Diffraction Xcalibur diffractometer, equipped with a CCD area detector Sapphire S and a graphite monochromator utilizing $Mo_{K\alpha}$ radiation ($\lambda = 0.71073$ Å). Suitable crystals were attached to glass fibers using perfluoropolyalkylether oil (ABCR) and transferred to a goniostat where they were cooled to 150 K for data collection. Software packages used: CrysAlis CCD for data collection, CrysAlis Pro for cell refinement and data reduction. The crystal structure was solved by Direct Methods and refined on F^2 using full-matrix least squares with SHELXL97. Absorption correction was done semi-empirically from equivalents. CCDC-910685 (K_2[**2b**]·6DMF·H_2O), CCDC-910686 (K_2[**2c**]·3DMF) and CCDC-910687 (K_2[**2a**]·4DMF·Et_2O·H_2O) contain the crystallographic data for this publication. These data can be obtained free of charge from The Cambridge Crystallographic Data Centre via www.ccdc.cam.ac.uk/data_request/cif. Selected data for K_2[Si–Ent]·4DMF·Et_2O·H_2O: single crystal of dimensions $0.62 \times 0.37 \times 0.26$ mm^3, $C_{46}H_{61}K_2N_7O_{21}Si$, $M_r = 1154.31$, orthorhombic, space group $P2_12_12_1$, $a = 12.2921(7)$, $b = 18.9949(13)$, $c = 23.5416(15)$ Å, $V = 5496.7(6)$ Å^3, $Z = 4$, $\rho_{calcd} = 1.395$ g cm^{-3}, $\mu = 0.276$ mm^{-1}, $F(000) = 2424$, $2\theta_{max} = 24.99°$, collected reflections 23040, unique reflections 9613 ($R_{int} = 0.1063$), restraints 805, parameters 850, S = 1.056, $R1$ ($I > 2\sigma(I)$) = 0.0874, $wR2$ (all data) = 0.1271, max./min. residual electron density 0.469/−0.607 e Å^{-3}. Selected data for K_2[Ge–Ent]·6DMF·H_2O: single crystal of dimensions $0.55 \times 0.18 \times 0.13$ mm^3, $C_{48}H_{65}GeK_2N_9O_{22}$, $M_r = 1270.88$, orthorhombic, space group $P2_12_12_1$,

$a=12.7262(9)$, $b=17.6723(14)$, $c=25.0846(16)$ Å, $V=5641.5(7)$ Å^3, $Z=4$, $\rho_{calcd}=1.496$ g cm^{-3}, $\mu=0.777$ mm^{-1}, $F(000)=2648$, $2\theta_{max}=25.00°$, 25511 collected reflections, 9896 unique reflections ($R_{int}=0.1147$), 0 restraints, 753 parameters, S = 1.062, $R1$ ($I>2\sigma(I)$) = 0.0919, $wR2$ (all data) = 0.1518, max./min. residual electron density 0.688/−0.522 e Å^{-3}. Selected data for K_2[Ti–Ent]·3 DMF: single crystal of dimensions $0.57\times0.39\times0.15$ mm^3, $C_{39}H_{42}K_2N_6O_{18}Ti$, $M_r=1008.89$, monoclinic, space group $P2_1$, $a=13.112(2)$, $b=10.0316(17)$, $c=16.932(2)$ Å, $\beta=94.844(16)°$, $V=2219.2(6)$ Å^3, $Z=2$, $\rho_{calcd}=1.510$ g cm^{-3}, $\mu=0.463$ mm^{-1}, $F(000)=1044$, $2\theta_{max}=24.99°$, 9151 collected reflections, 6693 unique reflections ($R_{int}=0.0603$), 331 restraints, 712 parameters, S = 1.058, $R1$ ($I>2\sigma(I)$) = 0.0876, $wR2$ (all data) = 0.1774, max./min. residual electron density 0.405/−0.386 e Å^{-3}.

[14] a) T. D. P. Stack, T. B. Karpishin, K. N. Raymond, *J. Am. Chem. Soc.* **1992**, *114*, 1512–1514; b) S. S. Isied, G. Kuo, K. N. Raymond, *J. Am. Chem. Soc.* **1976**, *98*, 1763–1767; c) J. V. McArdle, S. R. Sofen, S. R. Cooper, K. N. Raymond, *Inorg. Chem.* **1978**, *17*, 3075–3078.

[15] R. J. Abergel, A. M. Zawadzka, T. M. Hoette, K. N. Raymond, *J. Am. Chem. Soc.* **2009**, *131*, 12682–12692.

[16] a) W. R. Harris, K. N. Raymond, *J. Am. Chem. Soc.* **1979**, *101*, 6534–6541; b) W. R. Harris, C. J. Carrano, S. R. Cooper, S. R. Sofen, A. E. Avdeef, J. V. McArdle, K. N. Raymond, *J. Am. Chem. Soc.* **1979**, *101*, 6097–6104; c) L. D. Loomis, K. N. Raymond, *Inorg. Chem.* **1991**, *30*, 906–911; d) T. B. Karpishin, T. D. P. Stack, K. N. Raymond, *J. Am. Chem. Soc.* **1993**, *115*, 182–192; e) Z. Hou, T. D. P. Stack, C. J. Sunderland, K. N. Raymond, *Inorg. Chim. Acta.* **1997**, *263*, 341–355; f) B. P. Hay, D. A. Dixon, R. Vargas, J. Garza, K. N. Raymond, *Inorg. Chem.* **2001**, *40*, 3922–3935.

[17] a) J. J. Flynn, F. P. Boer, *J. Am. Chem. Soc.* **1969**, *91*, 5756–5761; b) P. Bindu, B. Varghese, M. N. S. Rao, *Phosphorus, Sulfur and Silicon* **2003**, *178*, 2373–2386.

[18] B. A. Borgias, S. R. Cooper, Y. B. Koh, K. N. Raymond, *Inorg. Chem.* **1984**, *23*, 1009–1016.

[19] Electronic binding energies are calculated by using the Amsterdam Density Functional package (ADF2012, SCM, Theoretical Chemistry, Vrije Universiteit, Amsterdam, The Netherlands, www.scm.com), BLYP/TZ2P with ZORA relativistic corrections; a) G. te Velde, F. M. Bickelhaupt, S. J. A. van Gisbergen, C. Fonseca Guerra, E. J. Baerends, J. G. Snijders, T. Ziegler, *J. Comput. Chem.* **2001**, *22*, 931–967; b) C. Fonseca Guerra, J. G. Snijders, G. te Velde, E. J. Baerends, *Theor. Chem. Acc.* **1998**, *99*, 391–403.

[20] Note that these energies are the purely electronic binding energies. Entropy and solvation effects are not included.

[21] $Ti(OiPr)_4$ is used in the experiment, instead of $Ti(OMe)_4$. In our conceptual model calculations, we ignore this detail for simplicity. Whereas the absolute energies will be slightly different, the main points of our reasoning will not be affected by this approximation.

[22] K. N. Raymond, C. Carrano, *Acc. Chem. Res.* **1979**, *12*, 183–190.

Received: May 13, 2013
Published online: July 2, 2013

